Atmospheric Research 291 (2023) 106801

Contents lists available at ScienceDirect

Atmospheric Research

journal homepage: www.elsevier.com/locate/atmosres

Assessing the performance of the HARMONIE-AROME and WRF-ARW numerical models in North Atlantic Tropical Transitions

C. Calvo-Sancho [a,*], L. Quitián-Hernández [a], J.J. González-Alemán [b], P. Bolgiani [c], D. Santos-Muñoz [d], M.L. Martín [a,e]

[a] Department of Applied Mathematics, Faculty of Computer Engineering, University of Valladolid, Segovia, Spain
[b] Agencia Estatal de Meteorología (AEMET), Department of Development and Applications, Madrid, Spain
[c] Department of Earth Physics and Astrophysics, Faculty of Physics, Complutense University of Madrid, Madrid, Spain
[d] Danmarks Meteorologiske Institut, Denmark
[e] Institute of Interdisciplinary Mathematics (IMI), Complutense University of Madrid, Madrid, Spain

ARTICLE INFO

Keywords:
Object-based verification
Tropical Transitions
North Atlantic basin
WRF
HARMONIE-AROME

ABSTRACT

Tropical cyclones (TCs) can develop as a result of the tropical transition (TT) process, which occurs when an extratropical cyclone (EC) begins to exhibit tropical characteristics, forming a TC. In this study, four TT processes that lead to a hurricane structure [Delta (2005), Ophelia (2017), Leslie (2018), and Theta (2020)] are evaluated using two high-resolution numerical models (WRF and HARMONIE-AROME). Both tracks and intensities of the cyclones are assessed by comparing the simulated minimum sea level pressure and maximum wind speed to an observational dataset. Moreover, a spatial verification is performed by comparing the MSG-SEVIRI brightness temperature (BT) and accumulated precipitation (IMERG) to the corresponding simulations accomplished by both models. Analyzing the track results, the WRF model, on average, outstands HARMONIE-AROME. However, it is the HARMONIE-AROME model that performs better than WRF when reproducing the intensity of these cyclones. Concerning the BT spatial validation, HARMONIE-AROME slightly outperformed WRF when reproducing the cyclone's structure but failed when simulating the BT amplitude. Besides, both models achieved a nearly perfect cyclone location. In terms of accumulated precipitation results, the HARMONIE-AROME model overestimates the larger structures while underestimating the smaller ones, whereas the WRF model underestimates the bigger structures, being poorly located by both models. Although it is difficult to establish which numerical model performs better, the overall results show an outstanding of the HARMONIE-AROME model over the WRF model when simulating TT processes.

1. Introduction

Based on their dynamic and thermal structure, cyclonic low-pressure systems in Northern Hemisphere are usually classified as extratropical, tropical, or subtropical cyclones. Extratropical cyclones (EC) are deep cold-core atmospheric systems usually developed in a vertically highly-sheared baroclinic environment, i.e., with significant horizontal temperature gradient and thermal wind, and are characterized by an asymmetric cloud pattern (Holton, 2004). On the other hand, TCs have a deep warm-core and are mostly developed in a barotropic environment (Charney and Eliassen, 1964; Wang and Wu, 2004), mostly depending on the latent and sensible heat fluxes released from the ocean (McTaggart-Cowan et al., 2013). Finally, STCs are characterized by sharing tropical and extratropical features and having a thermal hybrid structure (Evans and Guishard, 2009; Quitián-Hernández et al., 2016).

When an EC or STC acquires fully tropical characteristics it is known as a TT (Davis and Bosart, 2004). Despite considering TCs exclusive to tropical latitudes, a significant number of tropical cyclogeneses occurs in baroclinic regions with the presence of an upper-tropospheric low (Davis and Bosart, 2004; McTaggart-Cowan et al., 2013; Bentley and Metz, 2016). Moreover, there has been even more significant repercussions of TTs in the North Atlantic Basin since the 2000's (NATL). According to Galarneau et al. (2015), TTs generally develop in the western NATL due to being characterized by higher sea surface temperatures (SSTs) and lower vertical wind shear values. In contrast, the eastern NATL has a more baroclinically induced component that could

* Corresponding author.
E-mail address: carlos.calvo.sancho@uva.es (C. Calvo-Sancho).

https://doi.org/10.1016/j.atmosres.2023.106801
Received 19 January 2023; Received in revised form 11 April 2023; Accepted 8 May 2023
Available online 18 May 2023

limit the formation of TTs (Calvo-Sancho et al., 2022a). On the other hand, the inverse of a TT is an extratropical transition (ET) where a TC interacts with baroclinic instability and attains a frontal structure, a typical feature of ECs.

During a TT process, the low-pressure disturbances may develop a Shapiro-Keyser extratropical cyclone configuration, with its associated bent-back warm/occluded front that undergoes a warm seclusion process (Shapiro and Keyser, 1990; Hulme and Martin, 2009a, 2009b; Quitián-Hernández et al., 2020).These disturbances are more likely to form a TT when they develop in conjunction with low sea surface temperature (SST; McTaggart-Cowan et al., 2015) and moderate wind shear (McTaggart-Cowan et al., 2013). In fact, several studies (McTaggart-Cowan et al., 2013; Galarneau et al., 2015; Calvo-Sancho et al., 2022a) have established a strong relationship between TC development and an environment with moderate to strong baroclinicity and consequent vertical wind shear. This particular kind of TC development is related to STCs undergoing TTs (Davis and Bosart, 2004; Evans and Guishard, 2009; Hulme and Martin, 2009a, 2009b).

This study analyzes four TT processes over the NATL associated with the following TCs: Tropical Storm Delta [NOV. 2005], Hurricane Ophelia [OCT. 2017], Hurricane Leslie [SEP. 2018], and Tropical Storm Theta [NOV. 2020]. To this end, numerical simulations of two limited area and high-resolution numerical weather prediction models have been compared to observational data. The models used are The *HIRLAM-ALADIN Research on Mesoscale Operational Numerical weather prediction In Euromed - Applications of Research to Operations at Mesoscale* model (HARMONIE-AROME; Bengtsson et al., 2017) and The *Weather Research and Forecasting* model (WRF; Skamarock and Klemp, 2008).

The main objective of this work is to examine the ability of these two models when simulating the track, intensity, and other useful fields for the analysis of the thermodynamical and convective characteristics of the TTs, such as the brightness temperature (BT) or accumulated precipitation. The analysis will be carried out in two periods: pre-TT, comprising the days when the cyclone has not yet experienced a tropical cyclone characteristics, and post-TT, which encompasses the days when the cyclone has already acquired tropical cyclone structure.

This paper is organized as follows. Section 2 is devoted to describing the datasets, numerical model setups, and methodology. Results and discussion are included in Section 3. In particular, in Sections 3.1 and 3.2, the cyclone's track and intensity are respectively analyzed. The cyclones' intensity is assessed through the calculation of the maximum 10 m wind speed (SPD) and minimum sea level pressure (SLP) and compared to the observational HURDAT database (Landsea and Franklin, 2013). Lastly, Section 3.3 shows the results obtained from the spatial verification of BT and accumulated precipitation simulated by both models and compared to derived satellite products. Finally, Section 4 summarizes the main conclusions.

2. Datasets, setup, and methodology

2.1. Datasets

a. *ERA5 dataset*

The ERA5 global atmospheric reanalysis dataset (Hersbach et al., 2020; C3S, 2017) generated by the European Center for Medium-Range Weather Forecasts (ECMWF) has been used in this study as the initial/boundary conditions for the numerical model's simulations. This dataset has substantially higher temporal (hourly outputs) and spatial resolution (0.25° x 0.25°) than the former generation datasets: ERA-40 (Uppala et al., 2005) and ERA-Interim (Dee et al., 2011). Consequently, the ERA5 datasets ensure accuracy in climatological studies (Taszarek et al., 2020; Calvo-Sancho et al., 2022b) as well as considering it as initial conditions for numerical weather prediction (Alonso-González et al., 2021; Calvo-Sancho and Martín, 2021).

b. *Observational data*

In order to analyze the cyclones' track, the Atlantic basin hurricane "best track" database (HURDAT) from the National Hurricane Center (NHC) is used. Storm location and maximum winds are archived every 6 h (at 0000, 0600, 1200, and 1800 UTC; Landsea and Coauthors, 2004a, 2004b, 2008).

b.1. *Satellite MSG-SEVIRI BT*

In the last few decades the use of satellite products has become an essential tool for meteorological and climatological purposes (Levizzani and Cattani, 2019; Retalis et al., 2020). This fact is based on the difficulty of obtaining surface-based observational data in the vicinity of intense atmospheric systems leading to areas with scarce or missing data. Consequently, considering the advanced algorithms used for generating satellite products is possible to estimate useful fields for atmosphere analysis (Skofronick-Jackson et al., 2019; Retalis et al., 2020).

One of the satellite products used in this work to validate the numerical model's simulations is the SEVIRI (Spinning Enhanced Visible and InfraRed Imager) which is the main instrument of the Meteosat Second Generation (MSG) satellite platform. This satellite supplies data in four visible-near infrared (VNIR) and eight infrared (IR) channels (Aminou, 2002). The spectrum spans from 3.9 to 0.6 μm producing precise and extended data throughout the atmosphere which enhances the quality of the initial and boundary conditions in numerical weather prediction models (Pasternak et al., 1994). The SEVIRI satellite has 15 min of temporal resolution and 3 km of horizontal resolution at the nadir and ~ 5 km in the study area, with a sampling distance at the nadir of 1 km for the High-Resolution Visible (HRV) channel.

According to Bormann et al. (2014), the appropriate channels to identify the top cloud cover and surface temperatures are 8.7 μm, 10.8 μm, and 12.0 μm IR channels. Moreover, the 10.8 μm and 12.0 μm IR channels are considered especially sensitive to the existence of clouds (Bormann et al., 2014; Montejo, 2016). Therefore, the 10.8 μm longwave IR channel, related to the BT field, is selected in this study as observational data to validate the model outputs.

b.2. *NASA GPM IMERG accumulated precipitation*

One of the main impacts of extreme cyclones like those analyzed in this study is precipitation. As a consequence, there has been an increase in the last decade in the number of surveys evaluating the correct simulation of precipitation. As mentioned above, the difficulty of obtaining observational data in the vicinity of these extreme atmospheric systems makes the use of an efficient satellite precipitation product essential.

NASA Global Precipitation Measurement (GPM) mission is an international network of satellites that provides observational data on rain and snow across the globe in order to improve the understanding of the Earth's water cycle and to assist in refining simulations of extreme events. Moreover, the Integrated Multi-satellitE Retrievals for GPM (IMERG; Huffman et al., 2015) is an algorithm developed by NASA to estimate accumulated precipitation in most parts of the globe by combining information from the NASA-GPM satellite constellation. The IMERG precipitation estimates are obtained by combining all available passive microwave radiometer observations from the GPM constellation (Hou and Coauthors, 2014) and rain gauge data from about 16,000 sites worldwide (Huffman et al., 2015). The GPM IMERG is considered the most efficient satellite precipitation product to derive the precipitation extent, total volume, and duration (Levizzani and Cattani, 2019).

IMERG has a high spatial resolution of 0.1° x 0.1° every 30 min covering the whole globe. Depending on the user's demand there are three available IMERG runs, i.e., early, late, and final runs, with different latency and precision. The early run (IMERG-E) is available with a 6-h delay and it is used for real-time applications that use

geostationary infrared data at fine time scales (morphing technique; Joyce et al., 2004. Moreover, the late run (IMERG-L) is available with an 18-h delay and is mostly used for crop forecasting. It employs additional microwave observations to be used in the morphing techniques. The IMERG-E and IMERG-L runs are used for climatological purposes. The final run (IMERG-F) is available with a 4-month delay and is mostly used for research applications (Huffman et al., 2017). Moreover, the IMERG-F uses monthly gauge adjustments to reduce bias (Tan et al., 2017). In the current study, the IMERG-F Level 3 half-hourly (Version 6) product has been used to analyze the accumulated precipitation in the study area. To satisfy the three-hourly outcomes of each model, the accumulated precipitation was evaluated using a 3-h accumulation.

2.2. Numerical weather prediction models

a. *HARMONIE-AROME*

From January 1st, 2021, 26 Euro-Mediterranean National Met Services join their scientific research efforts toward developing the tools of excellence for Numerical Weather Prediction (NWP) on Limited Area Domains and enter into a large partnership: the consortium ACCORD (A Consortium for COnvection-scale modeling Research and Development). The HARMONIE-AROME model is a canonical system configuration developed mainly by HIRLAM countries inside this consortium. The full ACCORD NWP system is currently being developed along the three main model configurations, the so-called Canonical System Configurations (CSC): AROME (Termonia et al., 2018), HARMONIE-AROME (Bengtsson et al., 2017) and ALARO (Termonia et al., 2018).

The HARMONIE-AROME model is commonly used as an operational model limiting the use of its data and validation results to the public. Upon license request, the HARMONIE-AROME model has been used for academic and research purposes studies related to resolve, among others, convective phenomena that occurred in December 2013 over Iran's western mountainous areas (Neyestani et al., 2018), a heavy precipitation event that occurred on September 2009 in Turkey (Toros et al., 2018), the detection of poor-visibility episodes (Fernández-González et al., 2019), fog-forecasting ability (Román-Cascón et al., 2019), several mountain lee waves episodes located to the south-east of the Guadarrama mountain range on Spain (Díaz-Fernández et al., 2022) or the simulation of an STC that occurred in October 2014 near the Canary Islands (Quitián-Hernández et al., 2021).

In the current survey, the v43h2.1 cycle of the HARMONIE-AROME model has been used. Simulations are configured with a single domain of 2.5 km grid resolution, 65 hybrid sigma pressure levels, and a temporal resolution of 30 s (Bengtsson et al., 2017). Domains have been defined with 1000 × 1000 west-east and south-north grid points, respectively, centered on each analyzed cyclone. The initial/boundary conditions have been obtained from the ERA5 reanalysis. The HARMONIE-AROME model has a convection-permitting configuration and uses a non-hydrostatic spectral dynamical core with semi-Lagrangian and semi-implicit discretizations of the equations. Domain center changes depending on the simulated cyclone.

The HARMONIE-AROME model shares some of the physical parameterizations used in the AROME-France model (Seity et al., 2011), which was developed for the Meso-NH model by the French research community (http://mesonh.aero.obs-mip.fr/mesonh55). They share the Morcrette shortwave radiation scheme (Seity et al., 2011; Bengtsson et al., 2017) and the majority of the ICE-3 microphysics package (Lascaux et al., 2006; see documentation at: http://mesonh.aero.obs-ip.fr/mesonh/dir_doc/book1_m48_19jan2009/scidoc_p3.pdf). In terms of radiation, the ALARO model's ACRANEB2 radiation scheme (Geleyn et al., 2017) and the HIRLAM model's HLRADIA radiation scheme (Nielsen et al., 2014) are also available. Similarly, both models share the SURFEX surface parameterization scheme (Masson et al., 2013). This scheme, primarily developed by Météo-France, is constituted of several physical models for the land surface, urban areas, lakes, and oceans (Bengtsson et al., 2017). Besides, the HARMONIE-AROME model employs a different parameterization scheme for shallow convection than the one used in the AROME-France model (EDKF; Pergaud et al., 2009), known as EDMFm (de Rooy, 2014; Bengtsson et al., 2017). Unlike the AROME-France parameterization, EDMFm employs a dual flow-mass approach in which two updrafts are distinguished: a dry updraft that never reaches the Lifting Condensation Level(LCL), and a wet updraft that condenses and becomes a cloud (Bengtsson et al., 2017). Finally, HARATU (Bengtsson et al., 2017) is used for turbulence parameterization, which is based on the original scheme used for turbulence in the regional climate model RACMO (van Meijgaard et al., 2012), in conjunction with HARMONIE-AROME. For more information about the HARMONIE-AROME model configuration, please read Bengtsson et al. (2017).

b. *WRF*

The WRF model is a mesoscale, three-dimensional, non-hydrostatic finite-difference model designed and used in both operational forecasting and research (Skamarock et al., 2019). Developed primarily by the National Center for Atmospheric Research (NCAR), the WRF model is probably the most widely used numerical weather prediction model in the scientific community. This model is versatile and flexible as it allows its configuration to be modified according to the user's interest. It has a single code, a data assimilation system, and a software architecture that supports parallel computing and system extensibility, allowing it to be used both on supercomputer mainframes and on personal computers.

In this survey, the WRF model (v4.0.3), using the Advanced Research WRF (ARW) core, has been configured to resemble as closely as possible the configuration defined for HARMONIE. Consequently, a two one-way nesting with an outer domain of 7.5 km and an inner domain of 2.5 km of horizontal resolution is defined with 1000 × 1000 west-east and south-north grid points, respectively. Domains were centered on each analyzed cyclone and defined with 65 hybrid sigma pressure levels. Moreover, time steps were configured in adaptative mode. The WRF physics options were selected as those set up for the Hurricane research mode. Among others, it is remarked the use of the WRF Single-Moment 6-class (WSM6) (Hong and Lim, 2006) parameterization scheme for the microphysics options, the Dudhia (Dudhia, 1989) and RRTM schemes for the short and longwave radiation, respectively, and the YSU (Hong et al., 2006) scheme for the planetary boundary layer (PBL) option. Considering the specified 2.5 km horizontal resolution in this study, no cumulus parameterization scheme is used; therefore cloudiness is explicitly computed by the model. The use of convective parameterization schemes for the simulation of deep convective meteorological systems over high-resolution domains continues to be debatable (an extended discussion regarding this problem is found in Quitián-Hernández et al., 2021).

Finally, the integration period in both models (HARMONIE-AROME and WRF) is configured with an extension from 42 h before the time of the transition to 30 h after the TT. Doing so makes it, it is possible to analyze with sufficient margin the processes that take place before, during, and after the TT process.

2.3. Methodology

The cyclone track analysis has been focused on calculating the track distance error for both models comparing it to the HURDAT "best track" data. The cyclone intensity has been evaluated by calculating the maximum 10 m SPD within a 500 km radius centered on the cyclone and this latter variable and the minimum SLP throughout the entire cyclone for both models.

According to the methodology described in Díaz-Fernández et al. (2020), and Quitián-Hernández et al. (2021), an analysis has been carried out through the spatial calculation of several statistical indices to determine the model's skillfulness compared to the derived satellite

products. These skill scores have been determined for each grid point of the analyzed domain and for both evaluated periods: pre-TT and post-TT. The statistical indices used in this study are defined hereafter:

Mean:

$$Mean = \frac{\sum_{i=1}^{N} X_i}{N}$$

where X is the simulated (BT or IMERG) or observed data (MSG BT or GPM IMERG) for every time step (N) and specific grid point.

BIAS:

$$BIAS = \sum_{i=1}^{N} \left(X_{s,i} - X_{o,i}\right)$$

where Xs and Xo are simulated and observed data for every time step (N) and specific grid point, respectively.

Spatial Correlation Coefficient (R):

$$R = \frac{\sum_{i=1}^{N} \left(X_{s,i} - \overline{X_s}\right)\left(X_{o,i} - \overline{X_o}\right)}{\sqrt{\sum_{i=1}^{N} \left(X_{s,i} - \overline{X_s}\right)^2} \sqrt{\sum_{i=1}^{N} \left(X_{o,i} - \overline{X_o}\right)^2}}$$

where Xs and Xo are simulated and observed data for every time step and specific grid point, respectively.

Root Mean Square Error (RMSE):

$$RMSE = \sqrt{\left(\frac{(X_s - X_o)}{N}\right)^2}$$

Standard Deviation (STDDV):

$$STDDV = \frac{\sqrt{\sum_{i=1}^{N} (X_i - \overline{X_i})^2}}{N}$$

where N is the total number of grid points.

As cyclones do not only develop only vertically but also horizontally owing to convective propagation (Weisman and Klemp, 1982), their geographical distribution and severity are critical regarding potential socioeconomic repercussions. Therefore, proper spatial modeling becomes a critical goal to provide improved forecasts. That is the reason why it is crucial to use methods capable of analyzing the spatial distribution, position, and severity of the event since this kind of meteorological event develops not only in the vertical plane but also in the horizontal one. Several innovative methods for the verification of Quantitative Precipitation Forecasts (QPFs) have been developed (Davis et al., 2006 a, b; Früh et al., 2007). These methods distinguish diverse precipitation objects and assess the accuracy of their predictions.

2.3.1. SAL method

The SAL (Structure, Amplitude, Location) feature-based measurement is a verification method that is not only based on a direct attribution of forecasted objects to the observed ones (Wernli and Sprenger, 2007) but evaluates the level of quality of a particular field, taking into consideration its 'structure' (e.g. dispersed convective cells, frontal rain bands; Früh et al., 2007). Several studies have already used this kind of verification method. Hofmann et al. (2009) used SAL to differentiate between the best and worst prognosis of the COSMO model oriented to QPFs. SAL was also applied to rate the Swiss (Jenkner, 2008) and southern German (Zimmer et al., 2009) QPF quality. Furthermore, Früh et al. (2007) used the SAL diagrams to evaluate the accuracy of precipitation estimates obtained from satellites and local numerical weather prediction. Although SAL is typically used for precipitation analysis, it has been first employed in this study (to the author's knowledge) to compare BT simulations to satellite data, as was also done by Griffin et al. (2017). Herein, the SAL method has been applied to the comparison between the satellite BT and GPM-IMERG accumulated precipitation and compared to the corresponding WRF and HARMONIE-AROME model simulations. Besides, aspects of the structure (S), amplitude (A), and location (L) of precipitation in a given area are all taken into account independently by the SAL technique. The ACCORD-HARP R language package (Deckmyn, 2022) was used to compute the SAL measurement.

In the SAL method, the S-component represents the size and shape of the object and takes values between [−2,2], with the negative values too small and/or peaked objects and positive ones too large and/or flat. Furthermore, the A-component evaluates the total precipitation in a certain area. Like the S-component, the values of the A-component range between [−2, 2], with the negative values related to an underestimation of predictability and positive values to an overestimation. The 0 value for the S and A-components indicates the perfect structure and amplitude in comparison to the observations. Finally, the displacement of the predicted and observed objects in relation to their total center of mass is quantified by the L-component. The L-component values are indicated in the top left colour bar of each SAL diagram and range from 0 to 2, with again the 0 value the ideal value.

As an additional way to interpret the results, the main features of the SAL data distribution are analyzed to assess the simulations' accuracy. According to Cui and Liu (2021), model simulations can be accurately considered if the associated probability density curves show a symmetrical distribution with a small range, i. e., few outliers and as centered and concentrated as possible. In the current survey, violin plots are derived, considering both density curves and boxplots, for the BT and the accumulated precipitation (see Fig. 1A and B, respectively, in the Supplementary Material). The Mann-Whitney *U* test (Mann and Whitney, 1947) is used to assess whether the SAL components from both models are significantly different from each other or not. The Mann-Whitney U test is used to compare two populations to determine their independence. This is a nonparametric test that establishes that the two populations are identical under the null hypothesis. The employed *p*-value is 0.05.

2.3.2. FSS method

The Fractions Skill Score (FSS) is considered in the current survey since it is considered a robust neighborhood verification technique (Roberts and Lean, 2008; Roberts, 2008; Sokol et al., 2022). Herein, FSS is used to strengthen the spatial verification analysis. As done with SAL, the object-based FSS metric is employed to evaluate the effectiveness of the numerical weather prediction models' forecast (BT or accumulated precipitation, herein). According to Skok and Roberts (2016), the FSS could directly quantify the rain's positioning error. Besides, Sokol et al. (2022) remark that the FSS provides little information on quantitative accuracy. Moreover, Zhao and Zhang (2018) highlighted similarities between the FSS and the conventional correlation score. However, they recognized evident advantages as the FSS identifies variations in precipitation time series, mainly when evaluating severe rainfall. In the present survey, the FSS has been calculated for each cyclone separately (not shown) and on average for the BT and accumulated precipitation, dividing the computation into the pre-TT and post-TT periods (see Section 3.3).

The FSS is defined as a variation of the Brier Skill Score:

$$FSS = 1 - \frac{FBS}{FBSref}$$

where $FBS = \frac{1}{N}\sum_{i=1}^{N}(O_i - F_i)^2$ is the Fraction Brier Score (Brier, 1950), also known as the mean squared error (MSE), N is the number of pixels in the analyzed domain, O_i is the observation and F_i the forecast. As the MSE heavily depends on how frequently the event actually occurs, a different MSE skill score was computed considering a reference forecast with low skill (Roberts and Lean, 2008). The FBS used as reference (FBS_{ref}) is the largest FBS that can be computed and derived from the forecast and observed fractions, making it the worst possible FBS. The FBS_{ref} is defined as

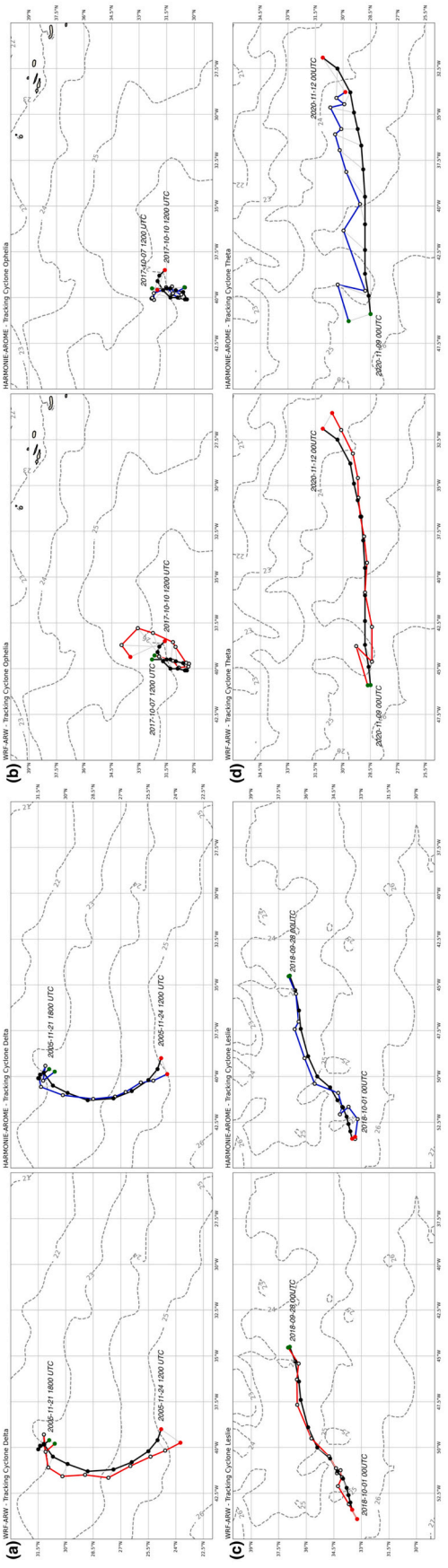

Fig. 1. Simulated tracks for WRF (red) and HARMONIE-AROME (blue) models against the HURDAT database (black) for a) Delta, b) Ophelia, c) Leslie and d) Theta. Data is displayed every 6 h. A green circle indicates the beginning of the track, while a red circle marks the end. (For interpretation of the references to colour in this figure legend, the reader is referred to the web version of this article.)

$$FBS_{ref} = \frac{1}{N}\left[\sum_{i=1}^{N} O_i^2 + \sum_{i=1}^{N} F_i^2\right]$$

The FSS takes values between 0 and 1, with 1 denoting the most accurate forecast. According to Roberts and Lean (2008), FSS values increase as the domain's square increases, implying that lower FSS values are obtained with finer numerical weather prediction resolution (Ebert, 2009).

3. Results and discussion

3.1. Track analysis

Following the above-mentioned methodology in Section 3.1, cyclone tracks from both the WRF and HARMONIE-AROME models have been analyzed for each cyclone and compare them to the HURDAT "best track" database (Fig. 1). Additionally, track distance errors have been calculated and averaged for the cyclones for each model (results of each cyclone in Supplementary Material), considering the pre-TT and post-TT periods when performing the analysis (Table 1).

Hurricane Delta track shows, in general, similar results depicted by both models compared to those shown by the HURDAT database (Fig. 1a). It is noteworthy that good results obtained by both models during the pre-TT, with a slightly more chaotic trajectory during the post-TT period. Ophelia's trajectory (Fig. 1b) displays more differences between models in contrast to the Delta's structure. While the HARMONIE-AROME model correctly simulates the track position, despite its chaotic evolution, the WRF model depicts a significantly deviated trajectory northeast in comparison to the HURDAT trajectory. Given the somewhat erratic simulated track of the system, it is difficult to perform an analysis for each defined period.

As occurred for Delta's trajectory, Leslie's track shows similar results by both models compared to the HURDAT track (Fig. 1c). Once again, both models produce better results during the pre-TT period than they do during the post-TT period. On the contrary, Theta's trajectory (Fig. 1d) exhibits a more dispersed trajectory. While HARMONIE-AROME does not correctly resolve the trajectory compared to the HURDAT track, the WRF model resolves a more consistent track compared to the HURDAT database (Fig. 1d). Furthermore, when evaluating the simulated track for each defined period, it is worth noting a slightly chaotic beginning of the pre-TT period by WRF. However, the model generates very good results from there to almost the end of the simulated trajectory, even coinciding with the observed tracking at some points. The HARMONIE-AROME model, on the other hand, depicts a more dispersed track throughout the entire simulation. All in all, Fig. 1 shows that, depending on the cyclone, each model reproduces the cyclone's track with greater or lesser accuracy. Averaged track distance errors show a WRF outperform against HARMONIE-AROME even with the smaller STDDV of the latter model.

3.2. Cyclone's intensity

In order to assess the WRF and HARMONIE-AROME's ability to resolve each cyclone intensity, maximum 10 m SPD and minimum SLP have been compared to the HURDAT database. The maximum 10 m SPD within a 500 km radius to the center of each cyclone is determined using

Table 1
Average track distance errors (km). The best results are highlighted in blue.

	Pre-TT		Post-TT	
Models	Average (km)	STDDV	Average (km)	STDDV
Harmonie-Arome	58	30	84	22
WRF	46	33	71	37

the Hart (2003) methodology when computing the Cyclone Phase Space diagrams. Analyzing the overall results (Fig. 2), the similarities found between both models throughout the simulated cycle are outstanding.

A general 10 m SPD overestimation is remarkable for both models. This positive bias is also found in Quitián-Hernández et al. (2021) in an STC that occurred in October 2014 in the vicinity of the Canary Islands. This STC is simulated with these same two numerical models finding higher values of SPD at lower atmospheric levels. Such overestimation is also observed in other studies (Kanase and Salvekar, 2014; Avolio et al., 2017) where the WRF model's YSU PBL parameterization scheme is used, as in the case. Lamraoui et al. (2018) attribute the WRF model's bias when simulating near-surface SPD to a lack of space (insufficient domain size) and time (insufficient spin-up), which might lead to a better simulation. In fact, computing the average and STDDV errors for the maximum SPD field considering all the TTs (Table 2), it is remarkable how good the results are shown by HARMONIE-AROME in comparison to the WRF model.

The evaluation of the minimum SLP for each cyclone during its entire cycle by the WRF and HARMONIE-AROME models (Fig. 2) provides information about the intensity of cyclones. Similar behavior is depicted by both models resolving the minimum SLP results for each analyzed cyclone (Fig. 2). A general overestimation is shown by both models compared to the HURDAT database, except for the Hurricane Delta, with a general underestimation during the entire simulation (Fig. 2a). Focusing on each model's results, it cannot be inferred which of the models excels in the ability to simulate the minimum SLP. However, as done for the maximum SPD, the average of the SLP difference and STDDV score is computed (Table 2) for each model, taking all the analyzed cyclones into account. Analyzing the results, once more, the HARMONIE-AROME outperforms the WRF model when simulating the minimum SLP.

3.3. Spatial verification

3.3.1. Standard skill scores

In this section, a spatial verification is carried out through the averaged calculation of the abovementioned spatial standard skill scores (mean, STDDV, BIAS, RMSE, and Pearson correlation coefficient) applied to the BT and accumulated precipitation fields. Firstly, the spatial verification is determined by comparing the SEVIRI observed 10.8 μm BT with the simulated BT by the WRF and HARMONIE-AROME models obtained from post-processing tools. Secondly, the accumulated precipitation obtained from the GPM-IMERG product is compared with the models' simulated field. The results are examined in light of the two analyzed periods: pre-TT and post-TT, encompassing the four analyzed cyclones (Delta, Ophelia, Leslie, and Theta). A summary of the spatial patterns of standard skill scores related to each system, obtained for the BT and accumulated precipitation, is available in the Supplementary Material.

A similar BT behavior is shown in both pre-TT (Fig. 3a) and post-TT periods (Fig. 3c), with better results obtained by the WRF model with fewer errors compared to HARMONIE-AROME. It should be noted that the discrepancies in the employed methodology to generate the models' BTs may also have an impact on the outcomes. Sokol et al. (2022) analyze pseudo-IR 10.8 μm ALADIN numerical weather prediction performance over a significant area of Europe during June 2020, obtaining greater biases versus SEVIRI BT data, as in this survey. These warm biases are also observed in Griffin et al. (2017) with a 3-km horizontal resolution Experimental High-Resolution Rapid Refresh model over the continental United States to simulate the BT field. Regarding the correlation results, it is the HARMONIE-AROME model that generally presents better outcomes for both analyzed periods (Fig. 3b and d).

Once the cyclones developed tropical features (post-TT period; Fig. 3d), both model correlation curves got increasingly distant from one another, with the HARMONIE-AROME model generating better results. These correlation coefficients resemble those found in Quitián-Hernández et al. (2021), whose analysis was also divided into two periods: pre-STC (when the cyclone is considered purely extratropical) and pure-STC (when the cyclone acquired a subtropical nature). Higher correlation results were found for HARMONIE-AROME when analyzing the BT in both the study by Quitián-Hernández et al. (2021) and the current survey. In addition, other studies (Díaz-Fernández et al., 2022) discovered a warm bias for the BT when evaluating several mountain wave episodes using the HARMONIE-AROME model.

The improvement of the BIAS and RMSE results compared to the BT in accumulated precipitation is remarkable (Fig. 4). HARMONIE-AROME displayed slightly better results for the RMSE score, but both models showed similar results for BIAS (Fig. 4a and c). The obtained dry results were also observed in Bagtasa (2021) in which a method was proposed for predicting accumulated TC rainfall from historical datasets using comparable TCs. Furthermore, Risanto et al. (2019) found that the configured convection-permitting WRF model failed to resolve convective processes during the 2017 North American Monsoon Season, resulting in a reduced precipitation rate and a drier bias. Risanto et al. (2019) used the GPM-IMERG product, similar to the one used in the current study to contrast the simulations and determined that the IMERG precipitation estimation is prone to uncertainties since it underestimates precipitation in comparison to rain gauge measurements. However, Yun et al. (2020) discovered a wet bias when simulating the 2008–2017 warm-season precipitation over Eastern China with the WRF model. As stated by Yun et al. (2020), some of the biases may be due to observational uncertainties, while some may be due to model deficiencies. A positive bias is also found in Armon et al. (2020) when performing a WRF simulation of heavy precipitation events over the Mediterranean Sea.

Since there is no bibliography on this subject for the HARMONIE-AROME model and given the very similar results obtained by both models, the WRF model will be used as a proxy to reference the results obtained by HARMONIE-AROME. Concerning the correlation results for the accumulated precipitation (Fig. 4b and d), both models again show similar results for both pre-TT and post-TT periods, with the HARMONIE-AROME's results distinguishing from those displayed by WRF. Once more, during the post-TT period (Fig. 4d) the correlation curves gradually diverge from one another.

3.3.2. SAL and FSS

The object-dependent SAL measurement is used because of its effectiveness in evaluating both large and small structures in simulations as a result of significant advances in numerical modeling that enable high-resolution simulations and thus the generation of finer structures. The SAL method also validates the object's location and intensity (Wernli and Sprenger, 2007; Früh et al., 2007). This method is herein applied to the BT and accumulated precipitation for both models. Additionally, the FSS skill score has also been calculated to spatially evaluate the models' ability to reproduce these fields to complement SAL. Once more, the results are presented by comparing both assessed periods (pre-TT and post-TT). To the author's knowledge, this is the first time that SAL and FSS are applied to the BT field.

Concerning BT, SAL results are relatively similar for both analyzed periods (Fig. 5). While smaller structures ($S < 0$) are generally obtained in comparison to the observation, the amplitude component is slightly underestimated ($A < 0$) for both models and periods (Fig. 5a and b). The A and S medians have been computed for the WRF and HARMONIE-AROME models (red and blue dashed lines, respectively, depicted in Fig. 5). Regarding median results of S during the pre-TT period (Fig. 5a), while both models show a negative structure median value, the HARMONIE-AROME model performs slightly better. Similar results are observed for both models when analyzing the amplitude median outcomes, with the WRF model outperforming the HARMONIE-AROME model. In terms of the location component, it is remarkable that both models have nearly perfect simulations (L-component median ~ 0.07) during the pre-TT and post-TT periods, with the HARMONIE-AROME

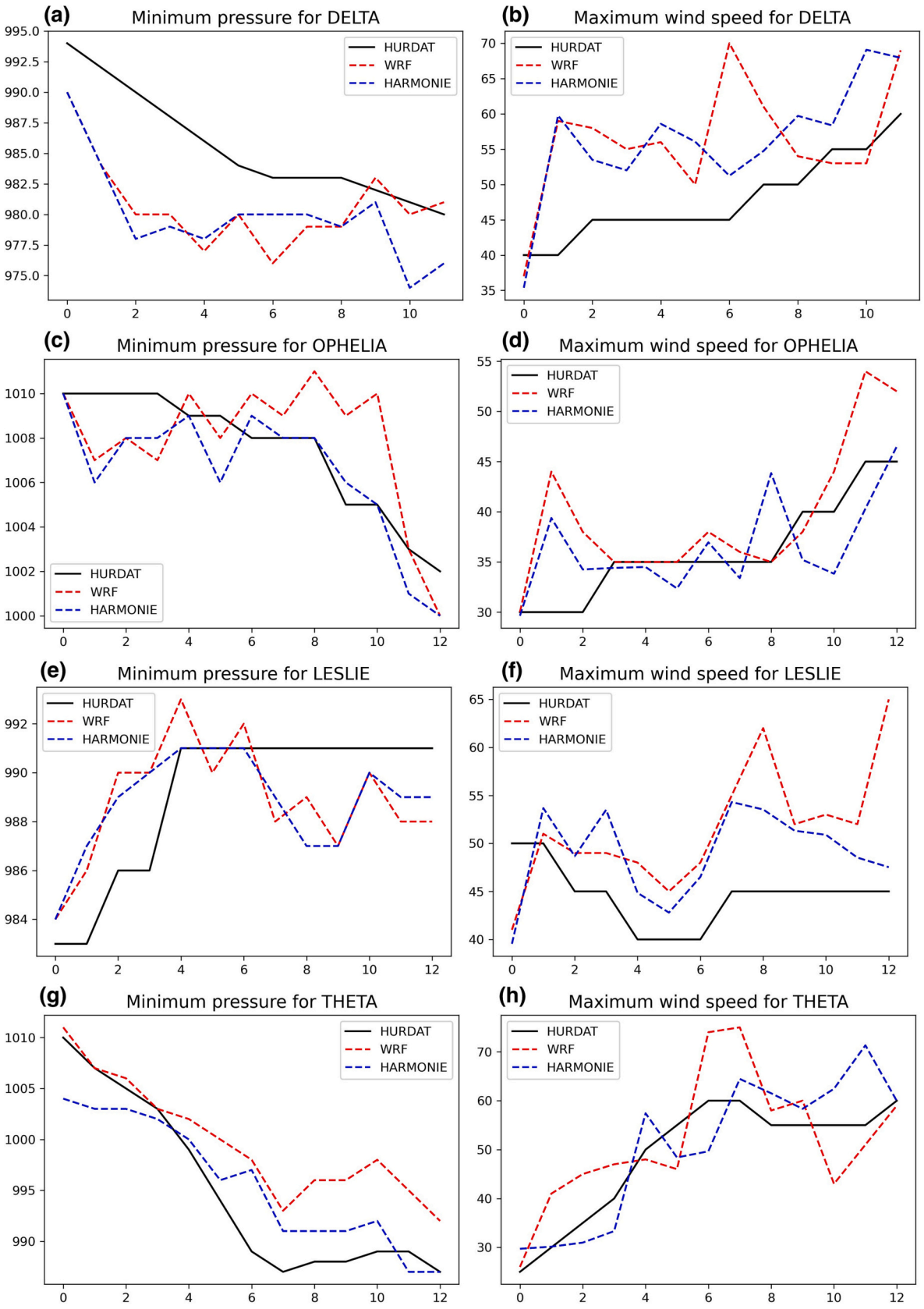

Fig. 2. Simulated minimum SLP (left) and maximum SPD (right) by WRF (red) and HARMONIE-AROME (blue) for a), b) Delta, c), d) Ophelia, e), f) Leslie and g), h) Theta. (For interpretation of the references to colour in this figure legend, the reader is referred to the web version of this article.)

Table 2
Averaged errors for SLP (hPa) and SPD (kts). The best results are highlighted in bold.

Average	SLP	SPD	STDDV	SLP	SPD
HARMONIE-AROME	**0.75**	**2.37**	HARMONIE-AROME	**2.68**	**6.39**
WRF	0.92	4.29	WRF	3.10	6.54

model (L-component median ~ 0.07) slightly better than WRF (L-component median ~ 0.08) during the latter period. During the pure TT period (Fig. 5b), the WRF model again yields slightly better median amplitude results. The structure median results are slightly worse than during the pre-TT period, but the behavior remains constant, i.e., both models simulate smaller structures (negative S values), and HARMONIE-AROME (blue dashed line) performs slightly better.

Concerning the statistical differences between the two models for the SAL components' distributions, it is outstanding that, while the A and L-components are statistically different (p-value <0.05), the S-component shows no significant differences (p-value >0.05). Besides, in general terms, both models depict a relatively symmetrical and concentrated distribution with few outliers (see Fig. 1A in the Supplementary Material). The WRF model depicts the range and a median closer to zero when simulating the A-component, implying a somewhat more accurate simulation than the one generated by HARMONIE-AROME; on the other hand, both models reproduce the S-component with similar results (see A and S-components in Fig. 1B of the Supplementary Material).

The FSS for BT is computed for both models and analyzed periods of all the TTs. Following Mazzarella et al. (2022) methodology, the FSS is determined in several moving spatial windows of increasing size. The FSS is computed in spatial windows of 2 km, 4 km, 8 km, 16 km, 32 km, and 64 km, considering four threshold values for the BT (233.15 K, 243.15 K, 253.15 K, and 263.15 K). A threshold of 240 K, chosen subjectively, was used for the calculation of the BT's SAL.

Recalling that the FSS values range from 0 to 1, with the latter being considered a perfect simulation, the computed BT averaged FSS values considering all TTs show that the HARMONIE-AROME model performs similarly to the WRF model when defining a window of 64 km. This is in agreement with the generally favorable results shown in the BT spatial pattern for HARMONIE-AROME, where the spatial pattern of clouds is remarkably similar to that of the SEVIRI satellite (see, for example, Fig. 2A, B, and D in the Supplementary Material). Moreover, the worse FSS values are obtained for the smallest 2 km window. These results are related to the fact that the larger the spatial window, the more objects are considered in the validation, resulting in a more accurate simulation (Mazzarella et al., 2022). Concerning the pre-TT period FSS results (top of Fig. 6) and considering that the best outcomes are obtained in the largest neighborhood window, WRF and HARMONIE-AROME yields similar outcomes (FSS ~ 0.43) when selecting a BT of 263.15 K and a 64 km window size. During the post-TT period (bottom of Fig. 6), HARMONIE-AROME (FSS ~ 0.43) outperforms WRF (FSS ~ 0.36) when selecting a BT of 263.15 K, maintaining a 64 km window.

Overall, the best FSS results are obtained when a 64 km neighborhood window is chosen. Concerning the results depicted by both models, while both models show similar results when choosing a BT of 263.15 K during the pre-TT period, HARMONIE-AROME outstands WRF during the post-TT period.

Regarding the precipitation field, during the pre-TT and post-TT periods Fig. 7 shows HARMONIE-AROME overestimation of larger precipitation structures ($A > 0$; $S > 0$) and overestimation of smaller ones ($A > 0$; $S < 0$) when compared to IMERG. On the other hand, WRF mostly overestimates the larger precipitation structures ($A > 0$; $S > 0$). Additionally, it is noticeable the overall spread displayed by both models, which is particularly clear in the HARMONIE-AROME case, given that it attains S values higher than 1. Finally, it is remarkable for both models that the larger simulated precipitation structures, compared to the observed ones, have a worse-positioned center of mass (L-component; Fig. 7). It is worth noticing that the S and A-component are significantly different (p-value <0.05), which is not the case for the L-component (see L-component in Fig. 1B of the Supplementary Material; p-value >0.05). Moreover, for the SAL components, models, and analyzed periods, it is remarkably the displayed symmetrical distribution. However, the HARMONIE-AROME appears to perform slightly

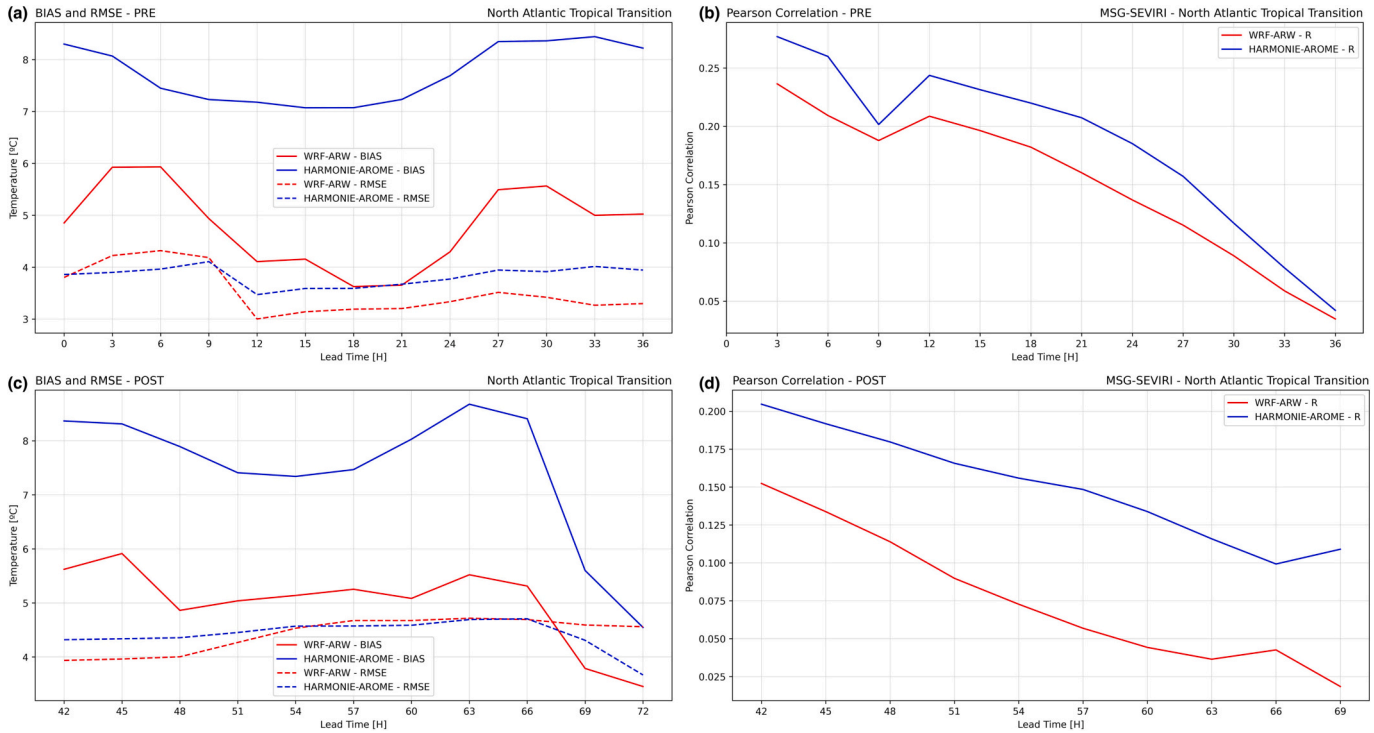

Fig. 3. Skill scores temporal evolution for BT for HARMONIE-AROME (blue) and WRF (red) models during the pre-TT (above) and post-TT period (below). (For interpretation of the references to colour in this figure legend, the reader is referred to the web version of this article.)

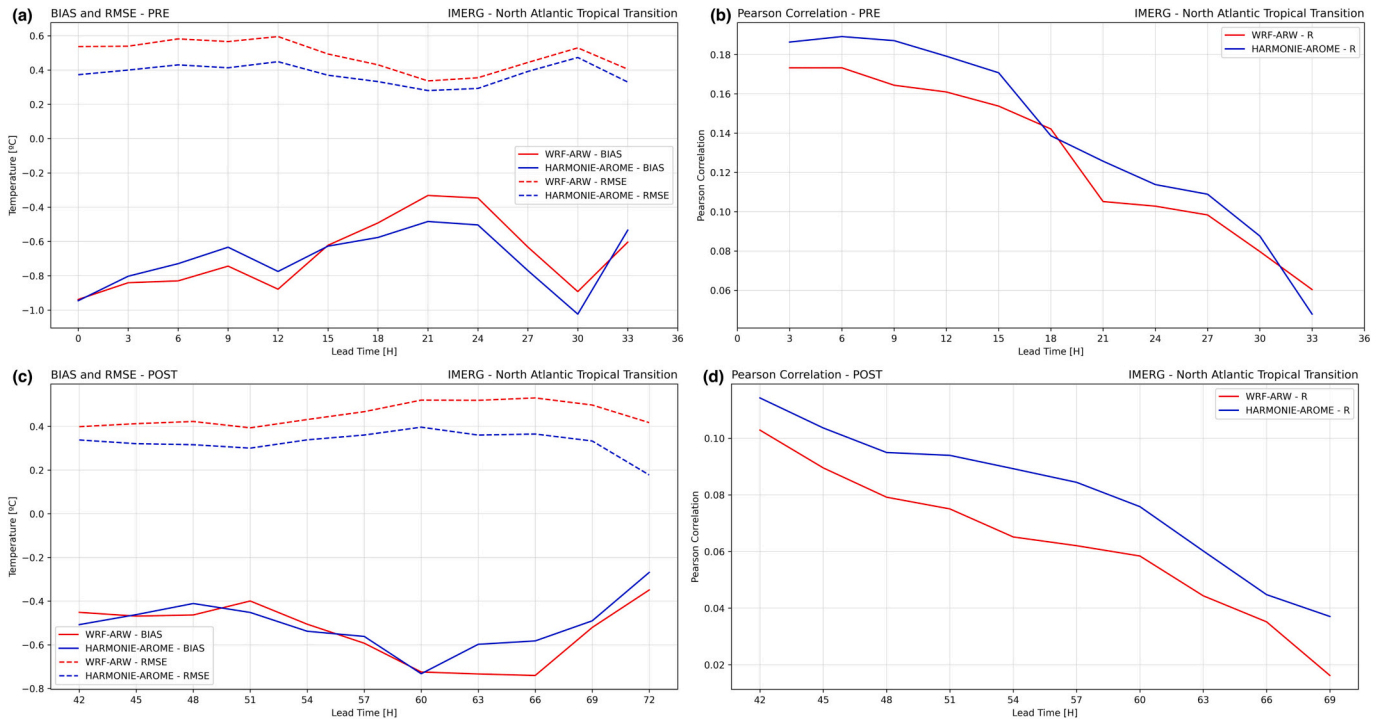

Fig. 4. Skill scores temporal evolution for accumulated precipitation for HARMONIE-AROME (blue) and WRF (red) models during the pre-TT (above) and post-TT period (below). (For interpretation of the references to colour in this figure legend, the reader is referred to the web version of this article.)

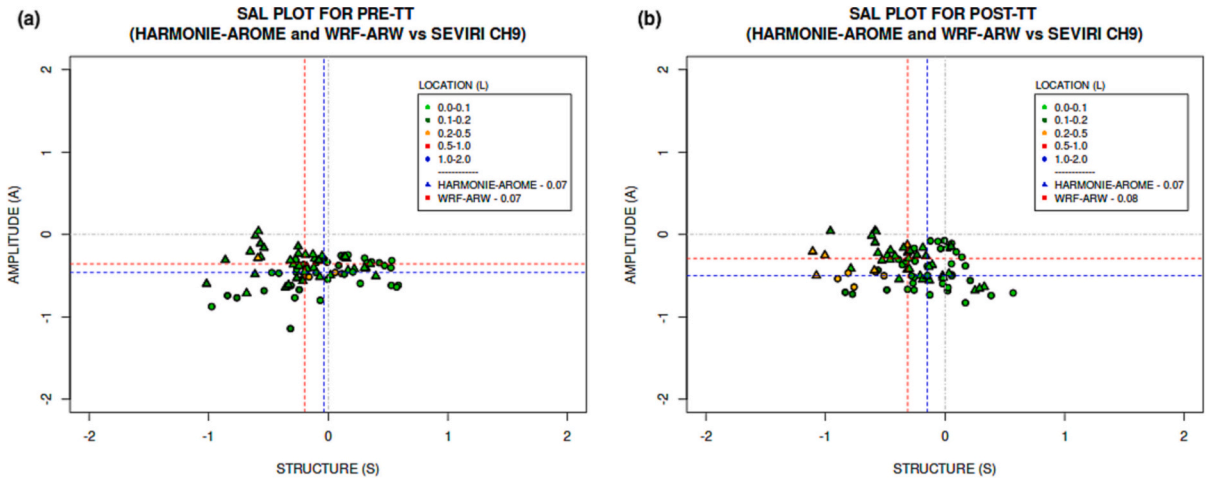

Fig. 5. HARMONIE-AROME (triangles) and WRF (circles) model SAL results for the BT field during the a) pre-TT and b) post-TT periods. The medians are displayed in dashed lines for HARMONIE-AROME (blue) and WRF (red). (For interpretation of the references to colour in this figure legend, the reader is referred to the web version of this article.)

better than WRF for both components (S and A) and in both analyzed periods since it displays the median closer to zero than that of WRF (see Fig. 1B in the Supplementary Material).

In a similar way as done for BT, the accumulated precipitation amplitude and structure medians have also been computed for both models and displayed in Fig. 7. During the pre-TT period (Fig. 7a), despite both models showing higher median structure values, HARMONIE-AROME performs slightly better than WRF. Moreover, in terms of amplitude, both models display relatively higher median values, with again the HARMONIE-AROME model outperforming the WRF. These results agree with the results obtained in the probability density function (see Fig. 1B in the Supplementary Material). Finally, concerning the location median outcomes, both models yield similar values (L-component median ~ 0.08).

Concerning the post-TT period (Fig. 7b), WRF median values for the A and S-components show similar results to those in the pre-TT time. The S - median value in the post-TT for HARMONIE-AROME (WRF) shows negative (positive) values, with the HARMONIE-AROME depicting the smaller distance obtained with regard to 0. Furthermore, regarding the A - median results for the HARMONIE-AROME model, an improvement (results closer to zero) is found in comparison to the pre-TT period data. Finally, in terms of location, HARMONIE-AROME (L-component median ~ 0.09) slightly stands out from WRF (L-component median ~ 0.11).

Additionally, the accumulated precipitation averaged FSS score is, once more, determined for both models and periods (Fig. 8). In this case, the neighborhood window sizes have been the same as those defined for the BT with the four selected thresholds for the accumulated

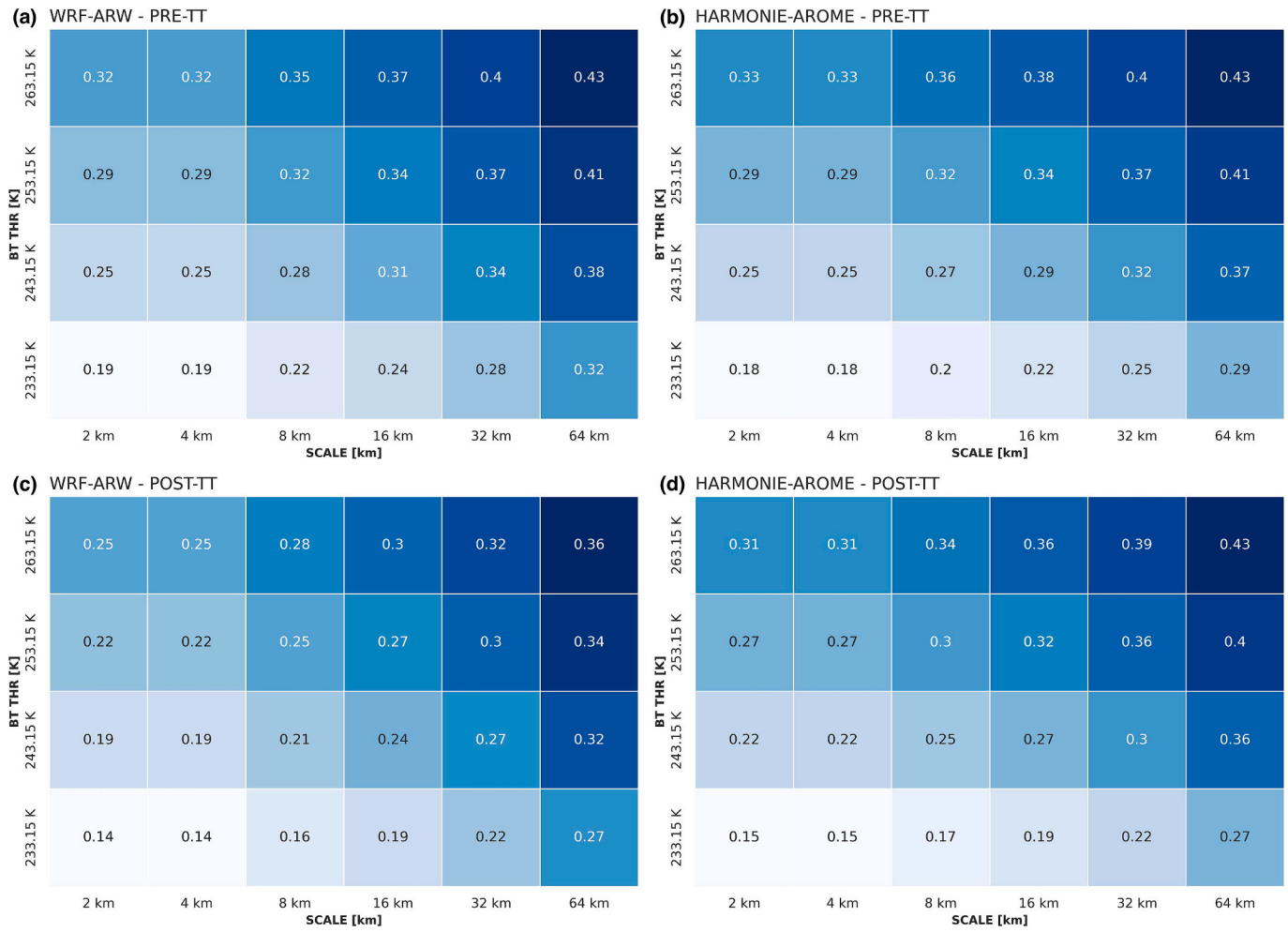

Fig. 6. BT averaged FSS considering all TTs for a), c) WRF, and b), d) HARMONIE-AROME during the pre-TT (above) and post-TT (below) periods.

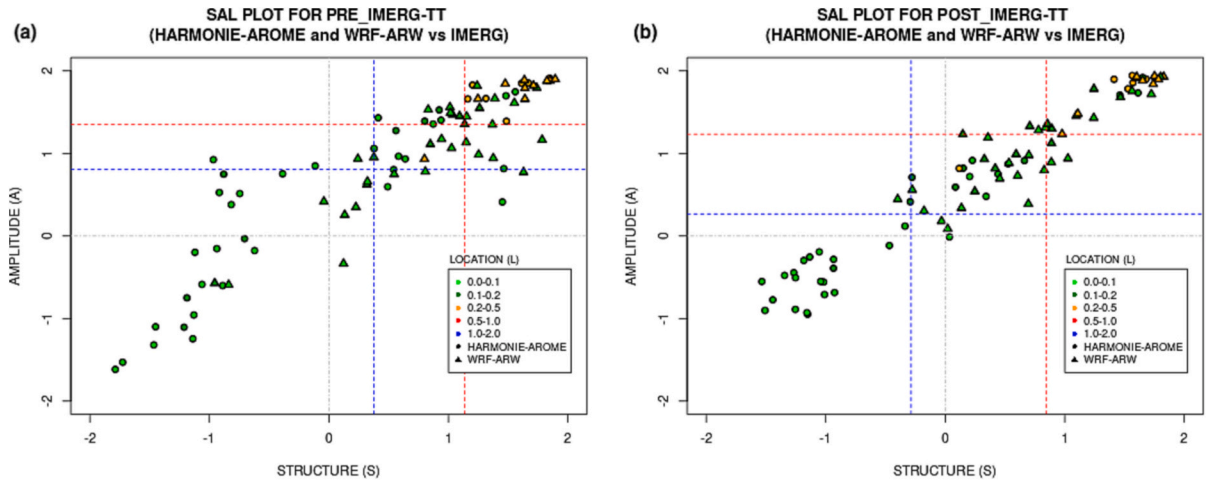

Fig. 7. HARMONIE-AROME (triangles) and WRF (circles) model SAL results for the accumulated precipitation field during the a) pre-TT and b) post-TT periods. The medians are displayed in dashed lines for HARMONIE-AROME (blue) and WRF (red). (For interpretation of the references to colour in this figure legend, the reader is referred to the web version of this article.)

precipitation being 5, 10, 20, and 40 mm, which comprise precipitation intensity from stratiform to convective or severe. The SAL computation concerning the accumulated precipitation employed a 15 mm threshold. Analyzing the results, both models depict similar results during the pre-TT and post-TT periods, with the WRF averaged FSS values slightly better during the pre-TT period (FSS ~ 0.38) and HARMONIE-AROME averaged FSS values better during the post-TT period (FSS ~ 0.47). The results indicate that the models accurately reproduce shallow or stratiform (~ 5–10 mm) precipitation but fail to simulate convective or severe precipitation (~ 40 mm). These results are in agreement with

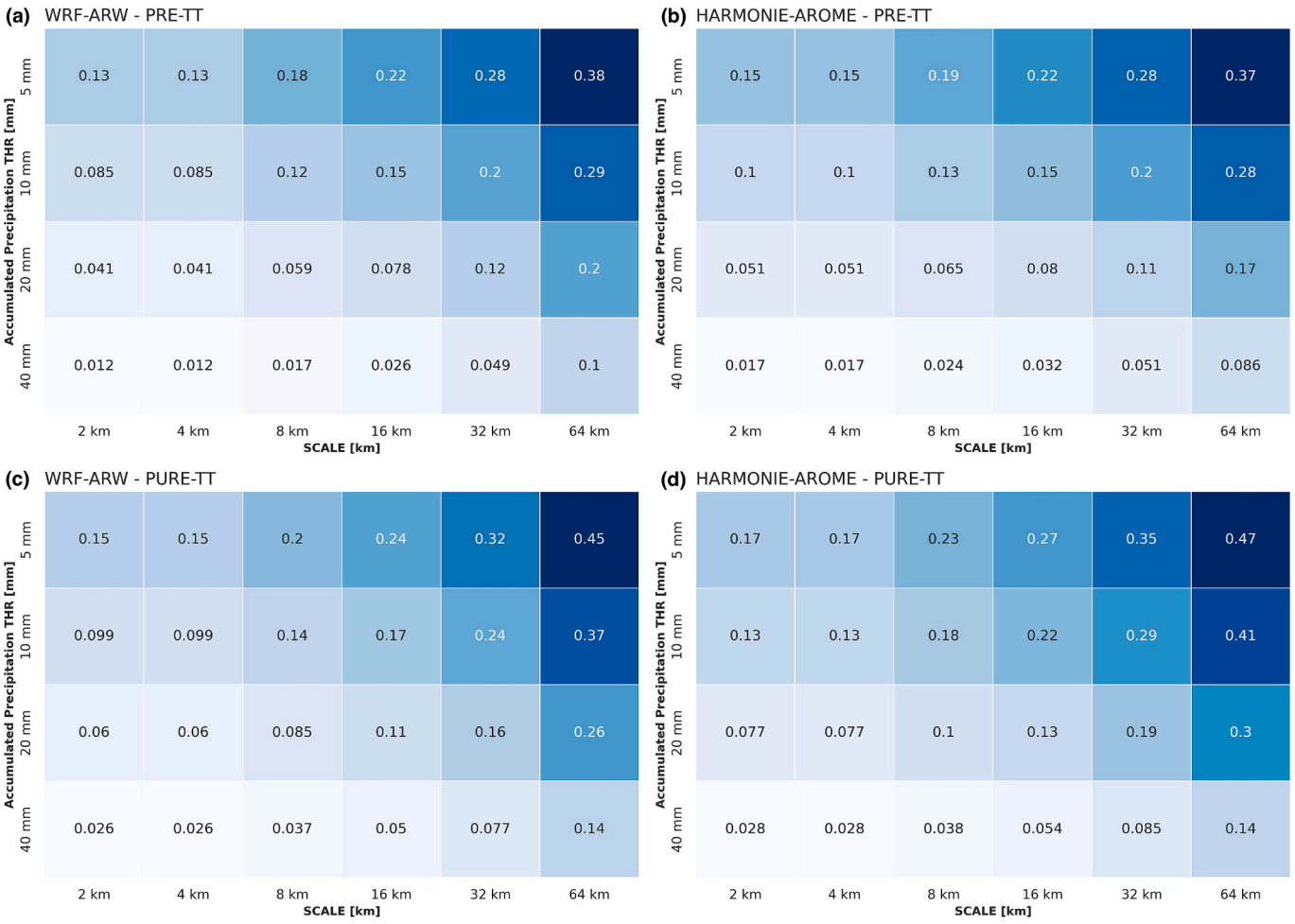

Fig. 8. Same as Fig. 6 except for the accumulated precipitation.

those shown in the spatial pattern of the accumulated precipitation (see Fig. 3A-D of the Supplementary Material related to each cyclone's results), where both models reproduce shallow precipitation, rather effectively as well as their horizontal distribution. Moreover, these obtained results are supported by Merino et al. (2022) where the WRF model best reproduced the stratiform events out of a total of 45 hourly precipitation events. As previously discussed in this study, Risanto et al. (2019) concluded that simulations performed by the WRF model configured for convection-permitting were unable to effectively resolve convective structures, which could explain the poor representation of convective precipitation shown in the results of the current work. Furthermore, the best averaged FSS outcomes were found for the largest 64 km window while the worst were obtained for the smallest 2 km window, which agrees with Mazzarella et al. (2022).

Overall, the averaged FSS values stand out in both analyzed periods, indicating that both models accomplish a very good simulation of the accumulated precipitation. Huang et al. (2020) emphasized the good results obtained from the simulation of the accumulated precipitation in terms of intensity and distribution when reproducing an extreme rainfall event in China using the WRF WSM6 microphysics scheme, as done in this survey. On the other hand, Hong et al. (2010) remarked that the double-moment microphysics scheme, such as the (WRF) Double-Moment 6-Class (WDM6; Lim and Hong, 2010) tends to improve the WSM6 deficiencies like suppressing spurious light precipitation. According to Hong et al. (2010), the WDM6 scheme presents a more realistic convective environment. Furthermore, Choi et al. (2018) demonstrated that double-moment schemes outperformed when extreme precipitation episodes associated with eight typhoons were simulated. However, some other authors (Huang et al., 2019) proved that using single-moment schemes provides a more accurate estimate of precipitation than using double-moment schemes. Recalling that, in this study, the WRF model was configured with the WSM6 microphysics scheme and due to the existing discrepancies in the use or non-use of one or the other scheme, further research is needed to understand the role of microphysics schemes in the representation of extreme precipitation.

Tables 3 and 4 show the SAL mean outcomes and FSS values for the BT and accumulated precipitation fields for both analyzed periods. The *p*-values for each SAL component and assessed field are likewise provided in the same SAL tables (see Fig. 1A and B in the Supplementary Material). Overall, both models performed similarly for the BT (Table 3) and accumulated precipitation (Table 4) fields throughout the pre-TT and post-TT periods. In terms of the SAL metric results (Table 3a), both models underestimate ($A < 0$) the smaller BT structures ($S < 0$), with the HARMONIE-AROME ($S = -0.03$) model slightly outperforming WRF ($S = -0.22$) when reproducing the BT object's structure and WRF ($A = -0.36$) surpassing HARMONIE-AROME ($A = -0.50$) when simulating the BT's amplitude. Regarding the SAL location, the WRF model ($L = 0.8$) slightly outstands the HARMONIE-AROME model ($L = 0.09$) during the pre-TT and post-TT periods. Moreover, regarding the p-values for the BT during both periods, while the amplitude and location are significantly different (p-value <0.05), the structure shows no significant differences (p-value >0.05). The FSS scores for both models and periods are remarkably similar, with the WRF model slightly outperforming HARMONIE-AROME.

Finally, when reproducing the accumulated precipitation, both models generally overestimate the larger precipitation structures

Table 3
a) SAL and b) FSS metric results for BT. Best results are highlighted in blue.

SAL - BT (p-value < 0.05)		S	A	L
PRE-TT	HARMONIE	-0.03	-0.50	0.09
	WRF	-0.22	-0.36	0.08
	p-value	0.39	0.00	0.02
POST-TT	HARMONIE	-0.19	-0.46	0.10
	WRF	-0.34	-0.32	0.12
	p-value	0.29	0.00	0.00

a

FSS - BT		FSS
PRE-TT	HARMONIE	0.37
	WRF	0.38
POST-TT	HARMONIE	0.45
	WRF	0.47

b

Table 4
Same as Table 3 except for the accumulated precipitation.

SAL - Accum. Pcp. (p-value < 0.05)		S	A	L
PRE-TT	HARMONIE	0.05	0.53	0.09
	WRF	0.99	1.16	0.11
	p-value	0.00	0.00	0.24
POST-TT	HARMONIE	-0.09	0.39	0.10
	WRF	0.86	1.17	0.13
	p-value	0.00	0.00	0.08

a

FSS - Accum. Pcp.		FSS
PRE-TT	HARMONIE	0.43
	WRF	0.43
POST-TT	HARMONIE	0.43
	WRF	0.36

b

(Table 4a), with the HARMONIE-AROME model with slightly better results during the pre-TT and post-TT periods. Whereas the S and A-component of the accumulated precipitation differ statistically (p-value 0.05), there are no significant differences in the location (p-value >0.05). The FSS score results yields similar results for the accumulated precipitation (Table 4b) during both analyzed periods, with outstanding outcomes when defining a wider neighborhood window. In the current paper, the FSS is used as it informs about the behavior of the models when simulating deep convection in TTs. FSS displays how the models fail to resolve the cyclones' convection dynamic at finer resolutions windows because of the convection processes involved in these energetic systems are complex, and the simulated rainfall patterns do not match the observational ones making low FSS values. The current FSS results have shown that the models are capable to resolve convective structures over 10–20 km. Moreover, this is related to the effective resolution of the models (Skamarock, 2004); in our case, the effective resolution is 17.5 km, obtained from 7Δx, being Δx the grid resolution for both models (Bolgiani et al., 2022; Calvo-Sancho et al., 2023) and indicating that both models are capable to resolve structures above 17.5 km and, therefore, showing better FSS results in larger resolutions windows.

4. Summary and conclusions

The main objective of this study is the analysis of four TT processes in the NATL corresponding to the cyclones [Delta (2005), Ophelia (2017), Leslie (2018), and Theta (2020)]. A series of simulations are carried out

for this aim, employing two high-resolution NWP models (WRF and HARMONIE-AROME). Results are validated by confronting the outputs with diverse observational and satellite data. First, the track of each of the cyclones is examined to assess the model's ability to simulate the evolution of the systems. Secondly, the intensity of these cyclones is examined throughout their evolution, assessing the SLP and SPD fields.

Finally, a spatial validation of two fields (BT and accumulated precipitation) related to their potential development is performed, given the spatial domain of the atmospheric systems. Both model simulations are tested against satellite datasets and several standard skill scores are calculated to perform a spatial analysis. The object-based SAL and FSS measures are also used to provide a more complete evaluation of cyclone distribution, position, and severity and, thus, to assess the accuracy of the models. The analysis is divided into two periods: pre-TT, the period prior to experiencing the TT, and post-TT, the period in which the cyclones have acquired tropical characteristics.

The main conclusions are summarized as follows:

- The computed averaged track errors for all analyzed cyclones show that the WRF model outperforms the HARMONIE-AROME model.
- A general overestimation from both models is obtained for the maximum 10 m SPD field compared to the HURDAT database, with the HARMONIE-AROME simulations slightly better, on average, in comparison to WRF. Both models' minimum SLP results show similar behavior for each cyclone. When compared to the HURDAT database, both models, except for Delta, overestimate the minimum SLP in all cyclones. Overall, after analyzing the average SLP for each model and taking all the TTs' SLP outcomes into account, the HARMONIE-AROME model outperforms the WRF model.
- The BT and accumulated precipitation field shows similar behavior in standard skills results by both models. However, the HARMONIE-AROME correlation results outstand those displayed by WRF for the BT and accumulated precipitation. The object-based verification displays similar BT results during both periods by the two models. HARMONIE-AROME and WRF resolve smaller structures and slightly underestimate. Regarding the location, both models have nearly perfect simulations. The FSS skill shows higher results in larger neighborhood spatial window. The WRF model performs slightly better in the pre-TT period and HARMONIE-AROME in the post-TT period.
- Regarding the object-based verification for accumulated precipitation field, the results and significant differences exhibit a general spread between both models. The HARMONIE-AROME overestimates the bigger precipitation structures while underestimating the smaller ones. The WRF model tends to overestimate the larger structures. The precipitation structures that were simulated to be bigger than observed have an inaccurate center of mass. The FSS skill displays similar results by both models. Both models reproduce stratiform precipitation more accurately than convective or severe precipitation. HARMONIE-AROME stands out from WRF during the pre-TT phase, whereas WRF outperforms HARMONIE-AROME during the post-TT period.

The current study's results underscore the utility of alternative validation techniques such as the SAL method or the FSS skill score for reproducing meteorological events that undergo a TT and for new fields, such as the BT. Based on the results, it is difficult to establish which numerical model performs better. Both models fare similarly when simulating the BT, and in terms of accumulated precipitation, both models reproduce stratiform precipitation more effectively than convective precipitation. Consequently, it is revealed as necessary to simulate more events related to TTs to study additional fields and results that give us a more detailed analysis to find out the causes of the differences/similarities between models.

CRediT authorship contribution statement

C. Calvo-Sancho: Conceptualization, Methodology, Software, Formal analysis, Writing – original draft. **L. Quitián-Hernández:** Conceptualization, Methodology, Software, Formal analysis, Writing – original draft. **J.J. González-Alemán:** Conceptualization, Methodology, Formal analysis. **P. Bolgiani:** Supervision. **D. Santos-Muñoz:** Supervision. **M.L. Martín:** Conceptualization, Methodology, Writing – review & editing, Supervision, Funding acquisition.

Declaration of Competing Interest

The authors declare that they have no known competing financial interests or personal relationships that could have appeared to influence the work reported in this paper.

Data availability

Data will be made available on request.

Acknowledgments

This work is supported by the Interdisciplinary Mathematics Institute of the Complutense University of Madrid. This work was partially supported by research project PID2019-105306RB-I00/AEI/10.13039/501100011033 (IBERCANES). This work is also supported by the ECMWF Special Projects SPESMART and SPESVALE. C. Calvo-Sancho acknowledges the grant awarded by the Spanish Ministry of Science and Innovation - FPI program (PRE2020-092343).

Appendix A. Supplementary data

Supplementary data to this article can be found online at https://doi.org/10.1016/j.atmosres.2023.106801.

References

Alonso-González, E., et al., 2021. Snowpack dynamics in the Lebanese mountains from quasi-dynamically downscaled ERA5 reanalysis updated by assimilating remotely sensed fractional snow-covered area. Hydrol. Earth Syst. Sci. 25, 4455–4471. https://doi.org/10.5194/hess-25-4455-2021.

Aminou, D., 2002. MSG's SEVIRI instrument. ESA Bull. 111.

Armon, M., Marra, F., Enzel, Y., Rostkier-Edelstein, D., Morin, E., 2020. Radar-based characterisation of heavy precipitation in the eastern Mediterranean and its representation in a convection-permitting model. Hydrol. Earth Syst. Sci. 24 (3), 1227–1249.

Avolio, E., et al., 2017. Sensitivity analysis of WRF model PBL schemes in simulating boundary-layer variables in southern Italy: an experimental campaign. Atmos. Res. 192, 58–71.

Bagtasa, G., 2021. Analog forecasting of tropical cyclone rainfall in the Philippines. Weather Clim. Extrem. 32, 100323.

Bengtsson, L., et al., 2017. The HARMONIE–AROME model configuration in theALADIN–HIRLAM NWP system. Mon. Weather Rev. 145, 1919–1935. https://doi.org/10.1175/MWR-D-16-0417.1.

Bentley, A.M., Metz, N.D., 2016. Tropical transition of an unnamed, high-latitude, tropical cyclone over the eastern North Pacific. Mon. Weather Rev. 144 (2), 713–736.

Bolgiani, P., Calvo-Sancho, C., Díaz-Fernández, J., Quitián-Hernández, L., Sastre, M., Santos-Muñoz, D., Martín, M.L., 2022. Wind kinetic energy climatology and effective resolution for the ERA5 reanalysis. Climate Dynamics 59 (3–4), 737–752.

Bormann, N., Hernandez-Carrascal, A., Borde, R., Lutz, H.-J., Otkin, J., Wanzong, S., 2014. Atmospheric motion vectors from model simulations. part i: methods and characterization as single-level estimates of wind. J. Appl. Meteorol. Climatol. 53 (1), 47–64. https://doi.org/10.1175/JAMCD-12-0336.1.

Brier, G.W., 1950. Verification of forecasts expressed in terms of probability. Mon. Weather Rev. 78, 1–3.

Calvo-Sancho, C., González-Alemán, J.J., Bolgiani, P., Santos-Muñoz, D., Farrán, J.I., Martín, M.L., 2022a. An environmental synoptic analysis of tropical transitions in the central and Eastern North Atlantic. Atmos. Res. 278, 106353.

Calvo-Sancho, C., Martín, Y., 2021. Supercell Pre-Convective Environments in Spain: A Dynamic Downscaling of ERA-5 Reanalysis, EGU General Assembly 2021, Online, 19–30 Apr 2021, EGU21–2967. https://doi.org/10.5194/egusphere-egu21-2967.

Calvo-Sancho, C., Díaz-Fernández, J., Martín, Y., Bolgiani, P., Sastre, M., González-Alemán, J.J., Martín, M.L., 2022b. Supercell convective environments in Spain based

on ERA5: hail and non-hail differences. Weather and Climate Dynamics 3 (3), 1021–1036.
Calvo-Sancho, C., Bolgiani, P., Subias, A., Sastre, M., González-Alemán, J.J., Martín, M. L., 2023. Horizontal kinetic energy analysis of tropical transition simulations with the WRF and HARMONIE-AROME Models. Q. J. R. Meteorol. Soc. Under review.
Charney, J., Eliassen, A., 1964. On the growth of the Hurricane depression. J. Atmos. Sci. 21 (1), 68–75.
Choi, Y., Shin, D.B., Joh, M., 2018. Assessment of WRF microphysics schemes in simulation of extreme precipitation events based on microwave radiative signatures. Int. J. Remote Sens. 39 (23), 8527–8551.
Cui, L., Liu, Z., 2021. Synergy between research on ensemble perception, data visualization, and statistics education: a tutorial review. Atten. Percept. Psychophysiol. 83, 1290–1311. https://doi.org/10.3758/s13414-020-02212-x.
Davis, C., Bosart, L., 2004. The TT problem: forecasting the tropical transition of cyclones. Bull. Am. Meteorol. Soc. 85, 1657–1662.
Davis, C.A., Brown, B., Bullock, R., 2006. Object-based verification of precipitation forecasts. Part I: methodology and application to mesoscale rain areas. Mon. Weather Rev. 134, 1772–1784.
de Rooy, W., 2014. The fog above sea problem: Part 1 analysis. In: Joint ALADIN-HIRLAM Newsletter, No. 2, Météo-France. Centre National de Recherches Meteorologiques, Toulouse, France, pp. 9–15. http://www.umr-cnrm.fr/aladin/IMG/pdf/ah_newsletter_2_april_2014_1_.pdf.
Deckmyn, A., 2022. harphub - A Part of the ACCORD Consortium [R HARP Spatial Verification – harpSpatial Package]. https://github.com/adeckmyn/harpSpatial.git.
Dee, D.P., et al., 2011. The ERA-Interim reanalysis: configuration and performance of the data assimilation system. Q. J. R. Meteorol. Soc. 137 (656), 553–597. https://doi.org/10.1002/qj.828.
Díaz-Fernández, J., Quitián-Hernández, L., Bolgiani, P., Santos-Muñoz, D., García Gago, Á., Fernández-González, S., Valero, F., Merino, A., GarcíaOrtega, E., Sánchez, J.L., Sastre, M., Martín, M.L., 2020. Mountain waves analysis in the vicinity of the Madrid-Barajas airport using the WRF model. In: Federico, S. (Ed.), Advances in Meteorology, 2020, p. 8871546. https://doi.org/10.1155/2020/8871546.
Díaz-Fernández, J., Bolgiani, P., Santos-Munoz, D., Quitián-Hernández, L., Sastre, M., Valero, F., Martín, M.L., 2022. Comparison of the WRF and HARMONIE models' ability for mountain wave warnings. Atmos. Res. 265, 105890.
Dudhia, J., 1989. Numerical study of convection observed during the Winter Monsoon Experiment using a mesoscale two–dimensional model. J. Atmos. Sci. 46, 3077–3107. https://doi.org/10.1175/1520-0469(1989)046<3077:NSOCOD>2.0.CO;2.
Ebert, E.E., 2009. Neighborhood verification: A strategy for rewarding close forecasts. Weather and Forecasting 24 (6), 1498–1510.
Evans, J., Guishard, M., 2009. Atlantic subtropical storms. Part I: diagnostic criteria and composite analysis. Mon. Weather Rev. 137 (7), 2065–2080. https://doi.org/10.1175/2009MWR2468.1.
Fernández-González, S., Bolgiani, P., Fernández-Villares, J., González, P., García-Gil, A., Suárez, J.C., Merino, A., 2019. Forecasting of poor visibility episodes in the vicinity of Tenerife Norte Airport. Atmos. Res. 223 (49–59), 2.
Früh, B., Bendix, J., Nauss, T., Paulat, M., Pfeiffer, A., Schipper, J.W., Thies, B., Wernli, H., 2007. Verification of precipitation from regional climate simulations and remote-sensing observations with respect to ground-based observations in the upper Danube catchment. Meteor. Z. 16, 275–293.
Galarneau, T.J., McTaggart-Cowan, R., Bosart, L.F., Davis, C.A., 2015. Development of North Atlantic tropical disturbances near upper-level potential vorticity streamers. J. Atmos. Sci. 72 (2), 572–597. https://doi.org/10.1175/JAS-D-14-0106.1.
Geleyn, J.F., Mašek, J., Brožková, R., Kuma, P., Degrauwe, D., Hello, G., Pristov, N., 2017. Single interval longwave radiation scheme based on the net exchanged rate decomposition with bracketing. Q. J. Royal Meteorol. Soc. 143 (704), 1313–1335.
Griffin, S.M., Otkin, J.A., Rozoff, C.M., Sieglaff, J.M., Cronce, L.M., Alexander, C.R., 2017. Methods for comparing simulated and observed satellite infrared brightness temperatures and what do they tell us? Weather Forecast. 32 (1), 5–25.
Hart, R.E., 2003. A cyclone phase space derived from thermal wind and thermal asymmetry. Monthly Weather Rev. 131 (4), 585–616.
Hersbach, H., et al., 2020. The ERA5 global reanalysis. Q.J.R. Meteorol. Soc. 146, 1999–2049. https://doi.org/10.1002/qj.3803.
Hofmann, C., Zimmer, M., Wernli, H., 2009. A brief catalog of poor and excellent COSMO model QPFs in German river catchments. In: Institut fu¨ r Physik der Atmospha¨re Internal Rep. 2. Universita¨ tMainz, 31 pp. [Available online at. http://www.staff.uni-mainz.de/zimmerm/catalogpoorexcellent.pdf.
Holton, J.R., 2004. An Introduction to Dynamic Meteorology. Academic Press (535 pp.).
Hong, S.-Y., Lim, J.-O., 2006. The WRF single-moment 6-class microphysics scheme (WSM6). J. Korean Meteor. Soc. 42 (2), 129–151.
Hong, S.-Y., Noh, Y., Dudhia, J., 2006. A new vertical diffusion package with an explicit treatment of entrainment processes. Mon. Weather Rev. 134, 2318–2341.
Hong, S.Y., Lim, K.S.S., Lee, Y.H., Ha, J.C., Kim, H.W., Ham, S.J., Dudhia, J., 2010. Evaluation of the WRF double-moment 6-class microphysics scheme for precipitating convection. Adv. Meteorol. 2010.
Hou, A.Y., Coauthors, 2014. The global precipitation measurement mission. Bull. Amer. Meteor. Soc. 95, 701–722. https://doi.org/10.1175/BAMS-D-13-00164.1.
Huang, Y., Liu, Y., Liu, Y., Li, H., Knievel, J.C., 2019. Mechanisms for a record-breaking rainfall in the coastal metropolitan city of Guangzhou, China: observation analysis and nested very large eddy simulation with the WRF model. J. Geophys. Res.-Atmos. 124 (3), 1370–1391.
Huang, Y., Wang, Y., Xue, L., Wei, X., Zhang, L., Li, H., 2020. Comparison of three microphysics parameterization schemes in the WRF model for an extreme rainfall event in the coastal metropolitan City of Guangzhou, China. Atmos. Res. 240, 104939.
Huffman, G.J., et al., 2015. NASA Global Precipitation Measurement Integrated Multi-satellitE Retrievals for GPM (IMERG). Algorithm Theoretical Basis Doc., version 4.5, 30 pp. [Available online at. http://pmm.nasa.gov/sites/default/files/document_files/IMERG_ATBD_V4.5.pdf.
Hulme, A.L., Martin, J.E., 2009a. Synoptic- and frontal-scale influences on tropical transition events in the Atlantic Basin. Part I: a six-case survey. Mon. Weather Rev. 137 (11), 3605–3625. https://doi.org/10.1175/2009MWR2802.1.
Hulme, A.L., Martin, J.E., 2009b. Synoptic- and frontal-scale influences on tropical transition events in the Atlantic Basin. Part II: tropical transition of Hurricane Karen. Mon. Weather Rev. 137 (11), 3626–3650. https://doi.org/10.1175/2009MWR2803.1.
Jenkner, J., 2008. Stratified Verifications of Quantitative Precipitation Forecasts over Switzerland. Ph.D. thesis,, vol. 17782. ETH Zurich, 98 pp.
Joyce, R.J., Janowiak, J.E., Arkin, P.A., Xie, P., 2004. CMORPH: A method that produces global precipitation estimates from passive microwave and infrared data at high spatial and temporal resolution. Journal of hydrometeorology 5 (3), 487–503.
Kanase, R.D., Salvekar, P.S., 2014. Study of weak intensity cyclones over Bay of Bengal using WRF model. Atmos. Clim. Sci. 4, 534–548.
Lamraoui, F., et al., 2018. The interaction between boundary layer and convection schemes in a WRF simulation of post cold frontal clouds over the ARM East North Atlantic site. J. Geophys. Res. Atmos. 124, 4699–4721. https://doi.org/10.1029/2018JD029370.
Landsea, C.W., Coauthors, 2004a. The Atlantic hurricane database re-analysis project: Documentation for the 1851–1910 alterations and additions to the HURDAT database. In: Murname, R.J., Liu, K.-B. (Eds.), Hurricanes and Typhoons: Past, Present and Future. Columbia University Press, pp. 177–221.
Landsea, C.W., Coauthors, 2004b. A reanalysis of Hurricane Andrew's (1992) intensity. Bull. Amer. Meteor. Soc. 85, 1699–1712.
Landsea, C.W., Coauthors, 2008. A reanalysis of the 1911–20 Atlantic hurricane database. J. Clim. 21, 2138–2168.
Landsea, C.W., Franklin, J.L., 2013. Atlantic hurricane database uncertainty and presentation of a new database format. Mon. Weather Rev. 141, 3576–3592.
Lascaux, F., Richard, E., Pinty, J.P., 2006. Numerical simulations of three different MAP IOPs and the associated microphysical processes. Q. J. R. Meteorol. Soc. 132 (619), 1907–1926.
Levizzani, V., Cattani, E., 2019. Satellite remote sensing of precipitation and the terrestrial water cycle in a changing climate. Remote Sens. 11, 2301.
Lim, K.-S.S., Hong, S.-Y., 2010. Development of an effective double-moment cloud microphysics scheme with prognostic Cloud Condensation Nuclei (CCN) for weather and climate models. Mon. Weather Rev. 138, 1587–1612.
Mann, H.B., Whitney, D.R., 1947. On a test of whether one of two random variables is stochastically larger than the other. Ann. Math. Stat. 18, 50–60.
Masson, V., et al., 2013. The SURFEXv7.2 land and ocean surface platform for coupled or offline simulation of earth surface variables and fluxes. Geosci. Model Dev. 6 (4), 929–960. https://doi.org/10.5194/gmd-6-929-2013.
McTaggart-Cowan, R., Galarneau Jr., T.J., Bosart, L.F., Moore, R.W., Martius, O., 2013. A global climatology of baroclinically influenced tropical cyclogenesis. Mon. Weather Rev. 141, 1963–1989. https://doi.org/10.1175/MWRD-12-00186.1.
Mazzarella, V., Milelli, M., Lagasio, M., Federico, S., Torcasio, R.C., Biondi, R., Parodi, A., 2022. Is an NWP-Based Nowcasting System Suitable for Aviation Operations? Remote Sensing 14 (18), 4440.
McTaggart-Cowan, R., Davies, E.L., Fairman Jr., J.G., Galarneau Jr., T.J., Schultz, D.M., 2015. Revisiting the 26.58C sea surface temperature threshold for tropical cyclone development. Bull. Amer. Meteor. Soc. 96, 1929–1943. https://doi.org/10.1175/BAMS-D-13-00254.1.
Merino, A., García-Ortega, E., Navarro, A., Sánchez, J.L., Tapiador, F.J., 2022. WRF hourly evaluation for extreme precipitation events. Atmos. Res. 274, 106215.
Montejo, I.B., 2016. Sensitivity study of the cloudiness forecast of the WRF model in the western half of Cuba. Rev. Cubana Meteorol. 22 (1), 66–80. https://doi.org/10.1155/2018/1381092.
Neyestani, A., et al., 2018. Inter-comparison of HARMONIE and WRF model simulations in convective-permitting scale over western area of Iran. Iran. J. Geophys. 12 (1), 1–18.
Nielsen, K.P., Gleeson, E., Rontu, L., 2014. Radiation sensitivity tests of the HARMONIE 37h1 NWP model. Geosci. Model Dev. 7, 1433–1449.
Pasternak, F., Lorsignol, J., Wolff, L., 1994. In: Cerutti-Maori, En G., Roussel, P. (Eds.), Spinning Enhanced Visible and Infrared Imager (SEVIRI): The New Imager for Meteosat Second Generation. https://doi.org/10.1117/12.185247.
Pergaud, J., Masson, V., Malardel, S., Couvreux, F., 2009. A parameterization of dry thermals and shallow cumuli for mesoscale numerical weather prediction. Bound. Layer Meteor. 132, 83–106.
Quitián-Hernández, L., Martín, M.L., González-Alemán, J.J., Santos-Muñoz, D., Valero, F., 2016. Identification of a subtropical cyclone in the proximity of the Canary Islands and its analysis by numerical modeling. Atmos. Res. 178, 125–137. ISO 690.
Quitián-Hernández, L., Bolgiani, P., Santos-Muñoz, D., Sastre, M., Díaz-Fernández, J., González-Alemán, J.J., Farrán, J.I., Lopez, L., Valero, F., Martín, M.L., 2021. Analysis of the October 2014 subtropical cyclone using the WRF and the HARMONIE-AROME numerical models: assessment against observations. Atmos. Res. 260.
Quitián-Hernández, L., González-Alemán, J.J., Santos-Muñoz, D., Fernández-González, S., Valero, F., Martín, M.L., 2020. Subtropical cyclone formation via warm seclusion development: The importance of surface fluxes. Journal of Geophysical Research: Atmospheres 125 (8), e2019JD031526.
Retalis, A., Katsanos, D., Tymvios, F., Michaelides, S., 2020. Comparison of GPM IMERG and TRMM 3B43 products over Cyprus. Remote Sens. 12 (19), 3212. https://doi.org/10.3390/rs12193212.

Risanto, C.B., et al., 2019. Evaluating forecast skills of moisture from convective-permitting WRF-ARW model during 2017 North American Monsoon season. Atmosphere 10, 694. https://doi.org/10.3390/atmos10110694.
Roberts, N., 2008. Assessing the spatial and temporal variation in the skill of precipitation forecasts from an NWP model. Met. Apps 15, 163–169. https://doi.org/10.1002/met.57.
Roberts, N.M., Lean, H.W., 2008. Scale-selective verification of rainfall accumulations from high-resolution forecasts of convective events. Mon. Weather Rev. 136, 78–97. https://doi.org/10.1175/2007MWR2123.1.
Román-Cascón, C., Yagüe, C., Steeneveld, G.-J., Morales, G., Arrillaga, J.A., Sastre, M., Maqueda, G., 2019. Radiation and cloud-base lowering fog events: Observational analysis and evaluation of WRF and HARMONIE. Atmos. Res. 229, 190–207. https://doi.org/10.1016/j.atmosres.2019.06.018.
Seity, Y., Brousseau, P., Malardel, S., Hello, G., Bénard, P., Bouttier, F., Lac, C., Masson, V., 2011. The AROME-France convective-scale operational model. Mon. Weather Rev. 139 (3), 976–991. https://doi.org/10.1175/2010MWR3425.1.
Shapiro, M.A., Keyser, D., 1990. Fronts, jets streams, and the tropopause. In: Newton, C. W., Holopainen, E. (Eds.), Extratropical Cyclones: The Erik Palmén Memorial Volume. American Meteorological Society, pp. 167–191.
Skamarock, W.C., 2004. Evaluating mesoscale NWP models using kinetic energy spectra. Mon. Weather Rev. 132, 3019–3032. https://doi.org/10.1175/MWR2830.1.
Skamarock, W.C., Klemp, J.B., 2008. A time-split non-hydrostatic atmospheric model for weather research and forecasting applications. J. Comput. Phys. 227 (7), 3465–3485. https://doi.org/10.1016/j.jcp.2007.01.037.
Skamarock, W.C., Klemp, J.B., Dudhia, J., Gill, D.O., Liu, Z., Berner, J., Huang, X.Y., 2019. A description of the advanced research WRF model version 4, 145. National Center for Atmospheric Research, Boulder, CO, USA, p. 550.
Skofronick-Jackson, G., et al., 2019. Satellite estimation of falling snow: a global precipitation measurement (GPM) core observatory perspective. J. Appl. Meteorol. Climatol. 58, 1429–1448.
Skok, G., Roberts, N., 2016. Analysis of fractions skill score properties for random precipitation fields and ECMWF forecasts. Quarterly Journal of the Royal Meteorological Society 142 (700), 2599–2610.
Sokol, et al., 2022. Evaluation of ALADIN NWP model forecasts by IR10.8 μm and WV06.2 μm brightness temperatures measured by the geostationary satellite Meteosat Second Generation. Atmos. Res. 265, 105920. ISSN 0169-8095. https://doi.org/10.1016/j.atmosres.2021.105920.
Tan, B.-Z., et al., 2017. Performance of IMERG as a function of spatiotemporal scale. J. Hydrometeorol. 18, 307–319. https://doi.org/10.1175/JHM-D-16-0174.1.
Taszarek, M., Allen, J.T., Púčik, T., Hoogewind, K.A., Brooks, H.E., 2020. Severe convective storms across Europe and the United States. Part II: ERA5 environments associated with lightning, large hail, severe wind, and tornadoes. J. Clim. 33, 10263–10286. https://doi.org/10.1175/JCLI-D-20-0346.1.
Termonia, P., Fischer, C., Bazile, E., Bouyssel, F., Brožková, R., Bénard, P., Joly, A., 2018. The ALADIN System and its canonical model configurations AROME CY41T1 and ALARO CY40T1. Geoscientific Model Development 11 (1), 257–281. ISO 690.
Toros, H., et al., 2018. Simulating heavy precipitation with HARMONIE, HIRLAM, and WRF-ARW: a flash flood case study in Istanbul, Turkey. Eur. J. Sci. Technol. 13, 1–12.
Uppala, S.M., et al., 2005. The ERA-40 re-analysis. Q.J.R. Meteorol. Soc. 131, 2961–3012. https://doi.org/10.1256/qj.04.176.
van Meijgaard, E., van Ulft, L., Lenderink, G., De Roode, S., Wipfler, E.L., Boers, R., van Timmermans, R., 2012. Refinement and application of a regional atmospheric model for climate scenario calculations of Western Europe. (inf.téc.). In: KVR Research Rep.
Wang, Y., Wu, C.-C., 2004. Current understanding of tropical cyclone structure and intensity changes–a review. Meteorog. Atmos. Phys. 87, 257–278. https://doi.org/10.1007/s00703-003-0055-6.
Weisman, M.L., Klemp, J.B., 1982. The dependence of numerically simulated convective storms on vertical wind shear and buoyancy. Monthly Weather Review 110 (6), 504–520.
Wernli, H., Sprenger, M., 2007. Identification and ERA-15 climatology of potential vorticity streamers and cutoffs near the extratropical tropopause. J. Atmos. Sci. 64 (5), 1569–1586. https://doi.org/10.1175/JAS3912.1.
Yun, Y., Liu, C., Luo, Y., et al., 2020. Convection-permitting regional climate simulation of warm-season precipitation over Eastern China. Clim. Dyn. 54, 1469–1489. https://doi.org/10.1007/s00382-019-05070-y.
Zhao, B., Zhang, B., 2018. Assessing hourly precipitation forecast skill with the fractions skill score. J. Meteorol. Res. 32, 135–145. https://doi.org/10.1007/s13351-018-7058-1.
Zimmer, M., Wernli, H., Frei, C., Hagen, M., 2009. Feature-based verification of deterministic precipitation forecasts with SAL during COPS. In: Proc. MAP D-PHASE Scientific Meeting, Bologna, Italy. Institute of Atmospheric Sciences and Climate and ARPA-SIM, pp. 116–121. Available online at. http://www.smr.arpa.emr.it/dphase-cost/master_proceeding_final.pdf.